Article

Cell Reports

Hierarchical retinal computations rely on hybrid chemical-electrical signaling

Graphical abstract

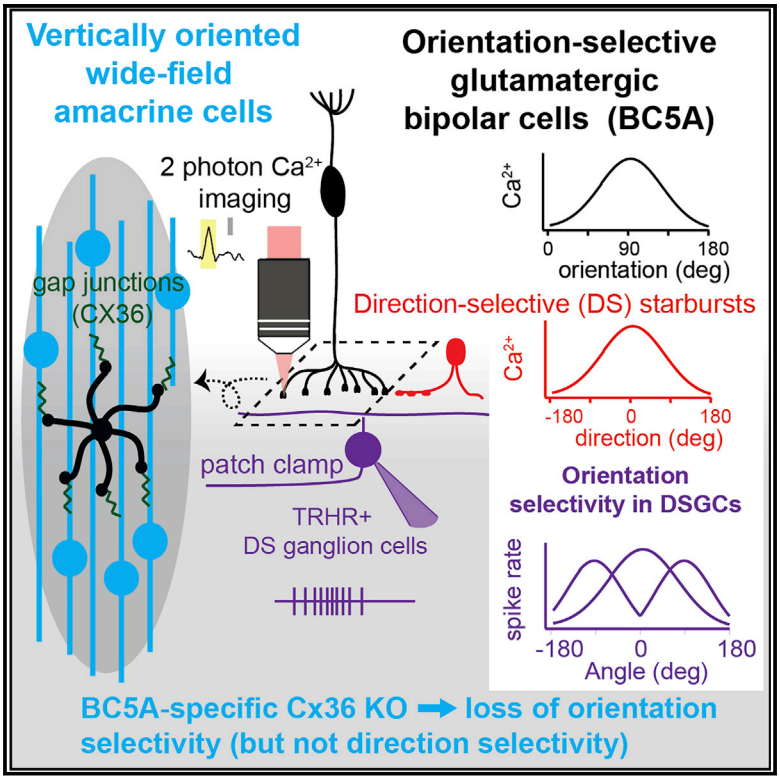

Highlights

- BC5A axon terminals respond best to vertically oriented features
- BC5A terminal orientation tuning relies on connexin 36-containing gap junctions
- Vertically orientated wide-field amacrine cell processes contact BC5A axon terminals
- BC5A tuning shapes orientation selectivity in postsynaptic DSGCs

Authors

Laura Hanson, Prathyusha Ravi-Chander, David Berson, Gautam B. Awatramani

Correspondence

gautam@uvic.ca

In brief

Hanson and colleagues demonstrate that glutamatergic excitatory inputs to classic ON-OFF direction-selective ganglion cells are tuned for orientation by being electrically coupled to a set of wide-field amacrine cells with vertically oriented processes. Thus, orientation and direction-selective information may be encoded by a single retinal neuron, like in the visual cortex.

Hanson et al., 2023, Cell Reports *42*, 112030
February 28, 2023 © 2023 The Authors.
https://doi.org/10.1016/j.celrep.2023.112030

CellPress

Cell Reports

CellPress
OPEN ACCESS

Article

Hierarchical retinal computations rely on hybrid chemical-electrical signaling

Laura Hanson,[1] Prathyusha Ravi-Chander,[1] David Berson,[2] and Gautam B. Awatramani[1,3,*]
[1]Department of Biology, University of Victoria, Victoria, BC V8W 3N5, Canada
[2]Department of Neuroscience, Brown University, Providence, RI 02912, USA
[3]Lead contact
*Correspondence: gautam@uvic.ca
https://doi.org/10.1016/j.celrep.2023.112030

SUMMARY

Bipolar cells (BCs) are integral to the retinal circuits that extract diverse features from the visual environment. They bridge photoreceptors to ganglion cells, the source of retinal output. Understanding how such circuits encode visual features requires an accounting of the mechanisms that control glutamate release from bipolar cell axons. Here, we demonstrate orientation selectivity in a specific genetically identifiable type of mouse bipolar cell—type 5A (BC5A). Their synaptic terminals respond best when stimulated with vertical bars that are far larger than their dendritic fields. We provide evidence that this selectivity involves enhanced excitation for vertical stimuli that requires gap junctional coupling through connexin36. We also show that this orientation selectivity is detectable postsynaptically in direction-selective ganglion cells, which were not previously thought to be selective for orientation. Together, these results demonstrate how multiple features are extracted by a single hierarchical network, engaging distinct electrical and chemical synaptic pathways.

INTRODUCTION

In the retina, light signals detected by photoreceptors are relayed to output ganglion cells via bipolar cells (BC), a diverse set of second-order excitatory interneurons. BCs serve to "filter" the neural representation of visual scenes formed by photoreceptors and create complex spatiotemporal patterns of activity in the inner retina.[1–3] This transformation serves as the first step in feature extraction, a process that enables a limited number of ganglion cells to efficiently relay visual information to higher brain centers.[4] Determining the precise types of operations carried out by different types of BCs is central to our understanding of how hierarchical networks in the retina process visual information.

BCs in mouse retina comprise ~15 types defined rigorously by a combination of functional, morphological, and/or molecular criteria.[1,4–7] Classic electrophysiological studies have shown that BCs have relatively simple concentric center-surround antagonist receptive field (RF) structures that differ in their size, polarity, and kinetics.[8–15] However, BC output is highly nonlinear due to the voltage-gated channels associated with transmitter release. This makes the axonal terminal a critical point of regulation central to many computations performed by amacrine cells in the inner retina.[16,17] For example, recent glutamate sensor imaging studies demonstrate that selectivity for features such as object direction and orientation, traditionally thought to be detected at the level of amacrine and ganglion cells, are already manifest in BC terminals.[18,19]

Determining how feature extraction occurs in the inner retina is not trivial, however, as BCs receive profuse electrical and chemical synaptic input at their axon terminals from diverse amacrine cells/and or other BCs. Previous studies have emphasized the role of inhibition of BC terminals, which is a powerful way that a huge variety of amacrine cells can control the spatiotemporal properties of BC output.[1,20–23] Alternatively, some amacrine cells, including the AII and A8 types, among others, provide excitatory signals to BC terminals via gap junctions. These may play specialized roles in the circuit.[24–27] In addition, gap junctions also appear to connect neighboring BCs, which appear to non-linearly affect spatial integration.[10,26,28–32] Finally, even once feature selectivity is realized at the level of individual BC terminals, understanding how this information is relayed to downstream ganglion cells has proven to be a challenge owing to uncertainties in the precise functional connectivity patterns[18,19]

In this study, we examined the functional properties of BCs that drive the direction-selective ganglion cell (DSGC) circuit in the mouse retina, focusing on type 5A BCs (BC5As; also referred to as BC5i[33]). BC5As can be genetically tagged in the KCNG4-Cre mouse line.[34] The glutamatergic input from BCs to DSGCs lacks any directional bias; direction selectivity originates instead primarily within the network of GABAergic/cholinergic starburst amacrine cells (starbursts[18,35–39]). We were thus surprised to find that BC5As encode the orientation of visual stimuli, apparently due to pronounced functional and anatomical asymmetries in the interactions with the network of wide-field (WF) amacrine cells. Convergent results from pharmacology and genetic knockout (KO) strategies as well as anatomical circuit tracing indicate that orientation selectivity in BC terminals arises through electrical coupling, possibly with a distinct type of wide-field

This is an open access article under the CC BY-NC-ND license (http://creativecommons.org/licenses/by-nc-nd/4.0/).

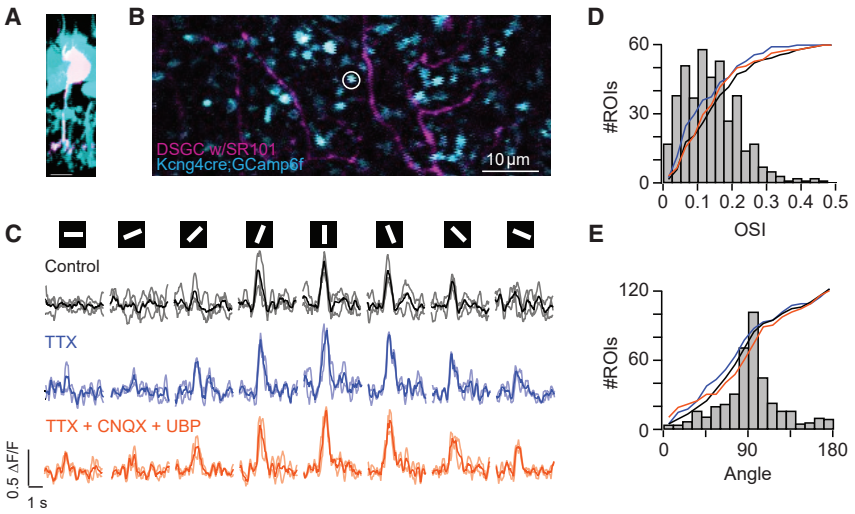

Figure 1. Orientation selectivity in type 5A bipolar cell axon terminals

(A) Confocal image of the fixed KCNG4-Cre × GcaMP6f mouse retina showing bipolar cells (BCs; cyan). An individual BC was loaded with Alexa 488 (white) using a sharp electrode prior to fixation.

(B) *En face* view of presumptive type 5A BC (BC5A) axon terminals (cyan) imaged in the living whole-mount KCNG4-Cre × GcaMP6f mouse retina using two-photon microscopy. BC terminals were imaged at the same depth in the inner plexiform layer as the ON dendrites of ON-OFF DSGCs (magenta, which was identified by their spiking properties and loaded with SR-101 prior to the imaging session). The circle indicates the example ROI for which light responses are shown in (C).

(C) Calcium responses from an example ROI (see B) evoked by static bars (50 × 500 µm, 8 orientations) illustrating orientation selectivity in BC terminals. Faint lines are individual trials, and dark lines are the average across 3–5 trials. Responses were measured under control Ringer's (black) or in drugs that are known to block spike-dependent wide-field GABA inhibition (TTX, blue) or most other types of feedforward and feedback inhibition (TTX + CNQX + UBP-310, orange).

(D) Distribution of OSI values across the population in control (n = 16 retina, 362 ROIs). Overlayed are the cumulative distribution for responses measured in control (black), TTX (blue), and TTX + CNQX + UBP-310 (n = 5 retina, 84 ROIs, same ROIs used for all conditions). TTX slightly reduced selectivity (control OSI = 0.16 ± 0.01; TTX OSI = 0.13 ± 0.009, $p < 0.05$), but this effect was lost in the added presence of CNQX + UBP-310 (OSI = 0.15 ± 0.01, $p = 0.3$).

(E) Distribution of angles across the population shows that most BCs have a strong preference for vertical bars (90°).

amacrine cell endowed with vertically oriented processes. Finally, we also investigated how these distinct properties of BC5As shape the responses of downstream DSGCs.

RESULTS

BC5As are tuned for vertically oriented stimuli

Functional imaging revealed that BC axon terminals respond most strongly to light bars that are vertically orientated in space (Figure 1). In these experiments, we imaged light-evoked changes in GCaMP6f signals in BC5A axon terminals labeled in the GCaMP6f × KCNG4-Cre mouse line (green channel).[34] These terminals arborized at the same depth within the inner plexiform layer as the ON dendrites of DSGCs (red channel; Figure 1B), which were loaded before the imaging experiment (see STAR Methods). Having a depth marker helped us exclude signals from dendrites of ON and OFF alpha ganglion cells, which also express GCaMP6f in the KCNG4-Cre mouse line.[40] The persistence of light-evoked Ca^{2+} signals in a cocktail of ionotropic glutamate receptor blockers that block ganglion cell responses also confirmed their presynaptic origin (Figure 1C). Finally, at the end of the imaging experiment, BC terminals were reconstructed within a small volume that captured the initial axon stalks to confirm their identity as BC5As (Figure 1A).

Individual BC terminals (Figure 1D) exhibited surprisingly strong orientation tuning as quantified using an orientation selectivity index (OSI; calculated as the vector sum of peak responses measured across 8 stimulus orientations; see STAR Methods). Tuning varied considerably across individual terminals, but most responded best to vertically oriented stimuli (Figures 1C–1E). These results are unexpected as previous studies have indicated that BC5As have a classic center-surround antagonistic RF organization responding strongly to stimuli presented over small circular areas (~50 µm in diameter) and exhibiting strong suppression by larger stimuli[1,41–44].

Amacrine cells with long, radially asymmetric processes oriented along the horizontal or vertical axes have previously been suggested to drive orientation selectivity in downstream retinal neurons (reviewed by Antinucci and Hindges[45]). Such asymmetric wide-field amacrine cells, through GABAergic synapses, could generate a postsynaptic preference for orientations perpendicular to the amacrine cell's (AC) biased anatomical orientation. On the other hand, excitatory electrical synapses might impose a preference for the AC's own orientation. To test whether inhibitory or excitatory mechanisms underlie orientation selectivity in BC5As, we next used a series of pharmacological manipulations to perturb select elements of the circuit.

First, we tested the effects of TTX, which blocks regenerative sodium currents and, thereby, the GABAergic inhibition from spiking wide-field ACs.[41,46] The effect is quite selective; TTX leaves release from BCs and other ACs relatively undisturbed. This abolished surround inhibition but only slightly reduced orientation selectivity (Figures 1C–1E and S1). We could not determine the tuning properties of the surround inhibition because inhibition cannot be observed consistently by calcium imaging; the voltage at BC terminals may often be subthreshold for activation of Ca^{2+} channels. Although we cannot rule out the possibility that orientation selectivity in BC5A terminals is partly shaped by GABAergic inhibition,[19] this inhibition does not appear to play an obligatory role in the process.

Next, we examined the additional effects of ionotropic glutamate receptor antagonists (50–100 µM CNQX and 10 µM UBP-310, which block AMPA and kainate receptors, respectively). This cocktail is expected to block feedforward and lateral inhibitory pathways mediated by a variety of types of ACs and

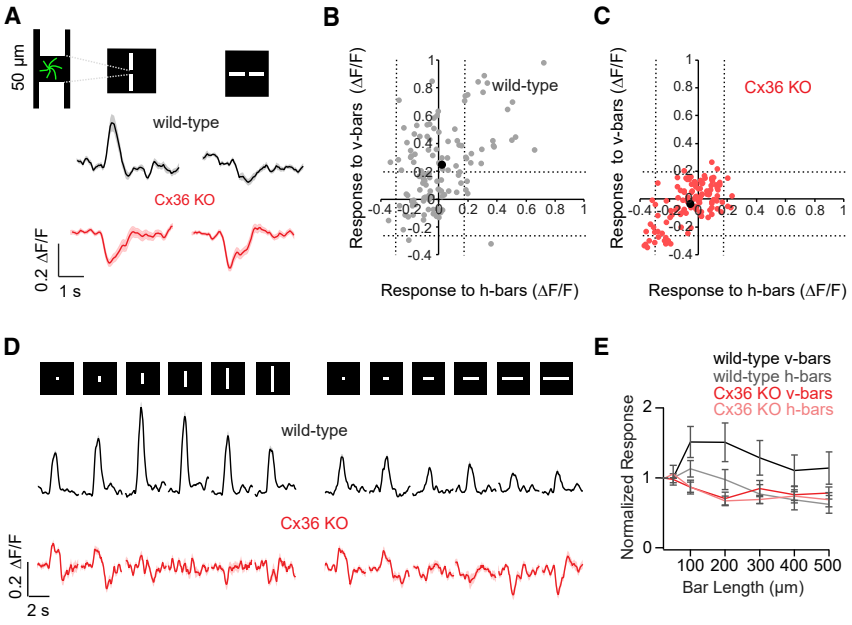

Figure 2. Connexin36-containing gap junctions are required for conveying remote excitation

(A) Robust calcium responses evoked from outside the BC's conventional excitatory receptive field (~size of its dendritic field). For remote stimulation, two bars, separated by a 50 µm gap, were placed along the vertical axis as schematized on the top left. By contrast, horizontal bars often caused a decrease in resting calcium, indicating the recruitment of wide-field inhibition (which was sensitive to TTX; Figure S1). In the BC5A-specific CX36 KO line (KCNG4-Cre × Gjd2$^{fl/fl}$), remote stimulation evoked inhibitory responses only (or no response at all).

(B and C) Peak response to remote stimulation in wild-type (B, n = 7) and CX36 KO retinas (C, n = 5). Dashed lines indicate 95% confidence interval for response distribution observed in the BC5A-specific CX36 KO retina.

(D) Responses to bars of different lengths placed along the vertical or horizontal axis shown for wild-type (black) and BC5A-specific CX36 KO (red) BCs (average response, dark; individual trials, light traces).

(E) Average peak responses to bars of different sizes in wild-type (n = 6) and in CX36 KO BCs (n = 5). Note that spatial integration beyond the BC center receptive field is only observed along the vertical axis in the wild-type retina. In the BC5A-specific CX36 KO retina, the optimal size of the stimulus matches the size of BC dendritic fields. Responses are normalized to those evoked by a small square (50 × 50 µm). Error bars represent ± SEM.

horizontal cells in the inner and outer retina, respectively, as well as a major component of the rod pathway mediated through the AII ACs.[24,46,47] In the presence of this cocktail of antagonists, the residual glutamatergic responses of ON BCs are presumably mediated by metabotropic glutamate receptor 6 (mGluR6[48,49]) expressed at their dendritic tips. These responses persisted but were often weaker than under control conditions, suggesting that the BC5A light response normally includes a contribution from the rod-AII amacrine-BC5A circuit. Consistent with this notion, the response amplitude could easily be recovered by increasing the stimulus intensity. Remarkably, under these reduced conditions, BC5As continued to exhibit robust orientation selectivity (Figure 1C). These findings demonstrate that the orientation selectivity in BC5A terminals is independent of direct or indirect ionotropic glutamate signaling pathways. This raises the interesting possibility that the mGluR-mediated ON signals generated in the dendrites of single BCs in the outer retina are re-shaped into orientation-selective (OS) signals by gap junction connections in the inner retina.

To test the coupling hypothesis further, we next examined whether BC terminals responded to stimuli outside the BC's classical RF (Figure 2). Indeed, we found that robust responses in BC5A terminals could be evoked even when a mask (~50 × 50 µm) was used to occlude the center RF to prevent the direct stimulation of BC dendrites in the outer retina (Figure 2A). On average, the surround responses were significantly stronger when stimuli were placed along the vertical compared with the horizontal axis. Importantly, surround excitation was not observed when the major gap junction protein expressed by BC5As (connexin36 [CX36][5]) was genetically knocked out specifically in BC5As (and possibly a few ganglion cells) using KCNG4-Cre × Gjd2$^{fl/fl}$ mice (Figure 2A). The ratio of the response evoked by vertical to horizontal bars was significantly higher in BCs measured in wild-type versus the BC5A-specific CX36-KO retina (Figures 2B and 2C). These results indicate that CX36-containing gap junctions mediate lateral excitatory signals to BC5A terminals.

In a separate series of experiments, we also measured the spatial area over which BC5As integrated information. In wild-type terminals, the peak amplitude of response continued to increase even when the bars were larger than their dendritic fields. For vertical bars, the optimal size was ~2–4 times the size of typical BC dendritic fields.[50] This elongation of the BC RF was significantly less pronounced when tested with horizontal bars. By contrast, BC5As lacking CX36 responded best to small spots that approximately matched the size of their dendritic fields (50 µm; Figure 2E). In these mutant retinas, longer bars often engaged the inhibitory surround, which manifested as light-evoked decreases in Ca^{2+} (Figure 2D). These results indicate that the extended spatial integrative properties of BC5As are highly reliant on CX36-mediated gap junction coupling.

Asymmetric wiring of the wide-field ACs to BC5A terminals

Electron microscopic analysis showed that orientation bias was also evident in the synaptic connectivity between wide-field AC and BC5A terminals. In a publicly available serial block-face electron microscopic volume of mouse inner plexiform layer,[51] we first identified large numbers of BC5As, based on their ribbon synaptic contacts onto DSGCs and starburst ACs, as previously described.[51] These BCs were distinguished from other

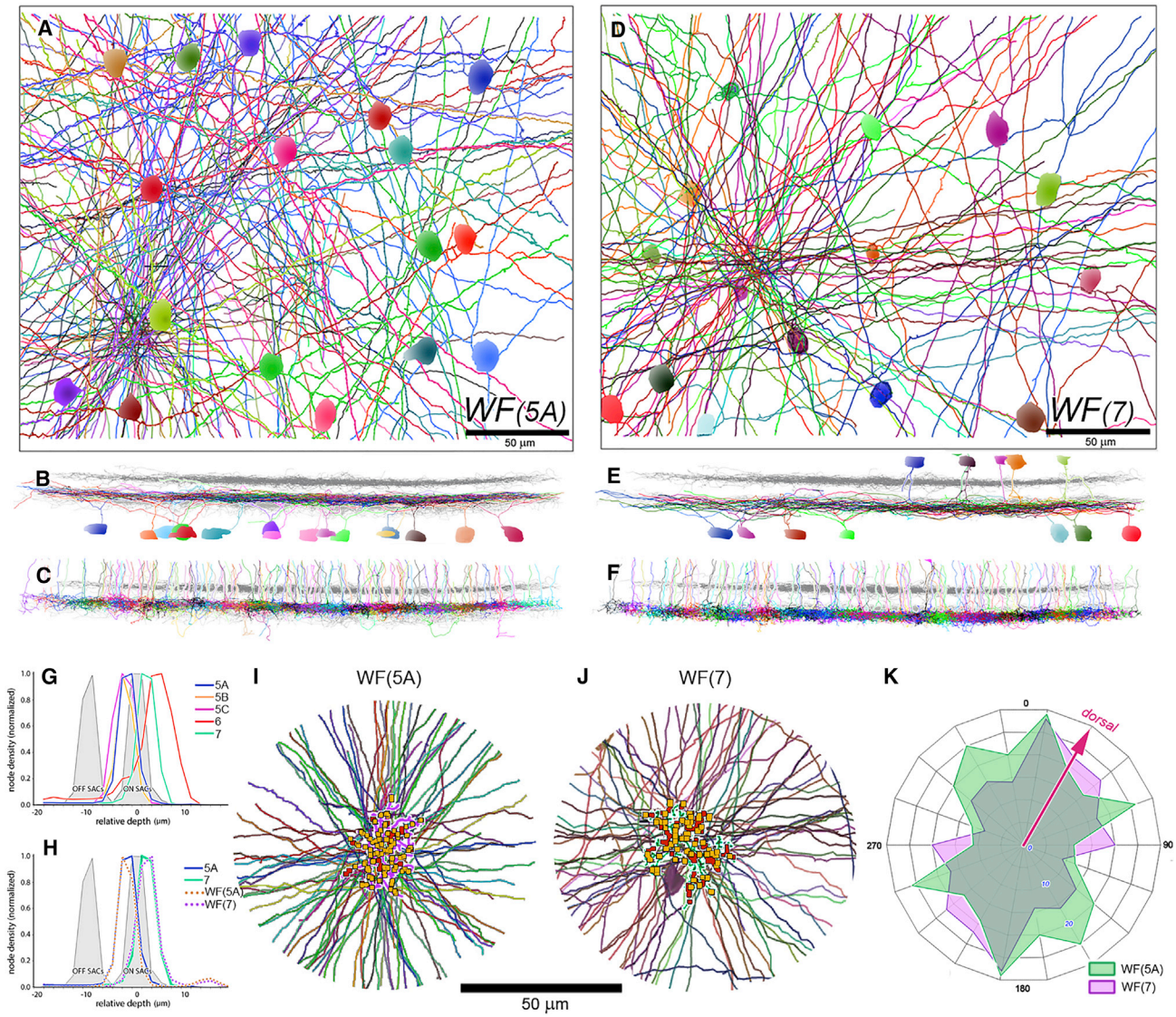

Figure 3. BC5A and BC7 axon terminals receive profuse synaptic contacts from specific types of wide-field amacrine cell types with asymmetric dendritic fields

(A) Top-down view of WF(5A) cells as viewed from the vitreal side. These cells were back traced from their postsynaptic contact points on BC5A terminals, the latter of which also serve as the dominant input source to WF(5A) (Table S1).

(B) Cross-sectional views showing the stratification of WF(5A) cell processes (colored profiles in A) with respect to the ON and OFF starburst plexuses (gray bands).

(C) Cross-sectional views showing the stratification of BC5A axon terminals in the same tissue block.

(D–F) WF(7) amacrine cells and their preferred bipolar target (BC7s), depicted for the panels just described (A–C).

(G) Depth profiles of selected BC types (BC solid lines) relative to the ON and OFF starburst processes (filled gray peaks).

(H) Close matches in stratification between WF(5A) amacrine cells and BC5A bipolar terminals and between WF(7) amacrine cells and BC7 terminals.

(I) Synaptic inputs from WF(5A) (small gold squares) onto a single BC5A terminal (pink). Red squares mark all other synaptic inputs to this terminal. The WF(5A) amacrine cells making these synapses are shown in the vicinity of the terminal.

(J) The BC7 terminal is shown in green, synaptic inputs from WF(7) cells are in gold, and other inputs are in red.

(K) Polar plots of the relative abundance of processes at specific orientations among WF(5A) amacrine cells (green) and WF(7) amacrine cells (purple). The dorsal-ventral axis was determined by the previously well-described asymmetric distributions of starburst and DSGC contacts as well as the asymmetric dendrites of specific retinal ganglion cells (see main text for details).

type 5B and 5C subtypes by their distinct stratification (Figures 3C and 3G) and the regular tiled mosaic formed by their terminal arbors.[33,51]

We then identified all conventional (non-ribbon) synaptic contacts onto BC5A terminals and traced the identified presynaptic partners. We found that the vast majority (50/55; 91%) derived

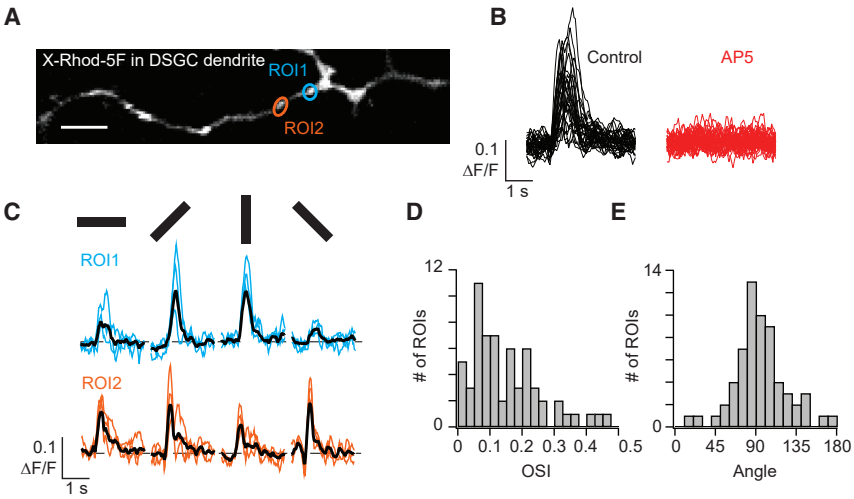

Figure 4. Glutamatergic inputs to DSGCs mediated by NMDA receptors are orientation selective

(A) Dendrite of a TRHR + DSGC filled with the red calcium indicator X-Rhod-5F. The DSGC was voltage clamped to 0 mV to relieve the Mg^{2+} block of NMDA receptors. Colored circles indicate the two example ROIs illustrated in (C). Scale bar, 5 μm.

(B) Calcium responses from 15 ROIs in control conditions or after application of the NMDA receptor antagonist (10 μM D-AP5).

(C) Two example ROIs show different levels of orientation selectivity in neighboring dendritic regions, indicating their relative independence.

(D and E) Distribution of OSI (D) and angles (E) calculated from peak ΔF/F values at individual ROIs (n = 5 DSGCs, 62 ROIs).

from what appeared to be a single wide-field amacrine type (Figures 3A–3C). These usually appeared as single, unusually straight processes that narrowly co-stratified with BC5A terminals (Figures 3A and 3H). Thus, AC input to BC5A terminals appears to be dominated by a single member of the class of GABAergic wide-field ACs,[52,53] which we thus refer to as WF5A.

Of the large numbers of synaptic contacts onto BC5A terminals, a few could be traced back to their parent cell bodies within the volume (Figure 3A). These exhibited a relatively regular spacing of cell bodies, typical of retinal mosaics formed by single-cell types. We also observed a few synapses on the BC5A axonal shaft, but owing to their sparsity, we did not analyze them further. BC5A terminals were the major synaptic target for these WF ACs as well as the main source of their excitatory ribbon synaptic input (Table S1), although other bipolar types stratifying at the same depth also provided some input.

Notably, these WF ACs exhibited a highly asymmetric distribution of orientations within the volume, with many more processes oriented along the dorsoventral (DV) axis of the retina than in other orientations (Figures 3I and 3K). The DV axis was inferred from the asymmetric dendritic fields of several types of ganglion cells[54,55] and was confirmed by asymmetric connectivity from starburst ACs to DSGCs.[51,56] This asymmetric distribution of WF amacrine processes contrasts with the symmetrical patterns of surround inhibition noted here and in previous studies (Figure 2F).[41] However, a similar analysis for BC7s revealed a near-identical asymmetric distribution of WF input from a distinct type of sparsely branching WF ACs (Figures 3D–3F, 3J, and 3K).

The skewed orientation distribution of WF processes aligns with the orientation preference of the BC5As that they target. Because the orientation selectivity of BC5As relies on electrical synapses as shown earlier, the oriented processes of WF ACs seem likely to confer orientation selectivity upon BC5As via electrical synapses (see discussion).

Orientation-selective responses in downstream ganglion cells

Our data do not provide direct evidence for orientation-selective glutamate release from BC terminals because GCaMP6f signals are highly non-linear and reflect only global Ca^{2+} levels in BC terminals. Furthermore, DSGCs and other targets of BC5A input may combine information from other BCs, possibly diluting OS tuning at the postsynaptic level. To address these issues, we next measured light-evoked NMDA receptor-mediated Ca^{2+} responses in dendrites of a single DSGC type—the posterior-motion-coding ON-OFF $TRHR^+$ DSGCs (p-DSGCs; Figures 4A–4C). These responses reflect the strength of individual BC inputs to DSGCs, including those from BC5As. To isolate NMDA receptor-mediated Ca^{2+} influx, DSGCs were voltage clamped at ~0 mV (cationic synaptic reversal potential; see STAR Methods), which served to relieve NMDA receptors from their Mg^{2+} block, inactivate voltage-dependent Ca^{2+} channels, and thereby minimize the potential for synaptic voltage escape.[57]

Under these conditions, robust Ca^{2+} signals were detected in "hot spots" (regions of interest [ROIs]) along the dendrites, presumptive sites of glutamatergic synaptic input. These responses could be blocked by the bath application of a selective NMDA receptor antagonist (50 μM D-AP5), confirming that the light-evoked Ca^{2+} signals were mediated by NMDA receptors. Approximately half of the ROIs were strongly tuned for orientation (36 of 62), and like the BC5A terminals, they responded best to vertically oriented bars (Figure 4D). Thus, optical imaging of NMDA receptor-mediated Ca^{2+} responses provided an independent verification that many BC inputs to DSGCs, some presumably from BC5As, are tuned for vertical orientation.

Orientation-selective information was also present in the spiking patterns of TRHR + p-DSGCs (Figure 5A). The strength of this orientation selectivity is comparable to that observed in the population of orientation-selective ganglion cells (OSGCs) of the mouse retina[58] (Figures 5E and 5H). Additionally, robust orientation selectivity was observed when pharmacological manipulations were used to disrupt direction selectivity mediated by starburst ACs. Specifically, when starburst output was blocked using DCG-IV,[59] direction selectivity was completely abolished, while orientation selectivity remained intact (Figures 5B, 5F, and 5H).

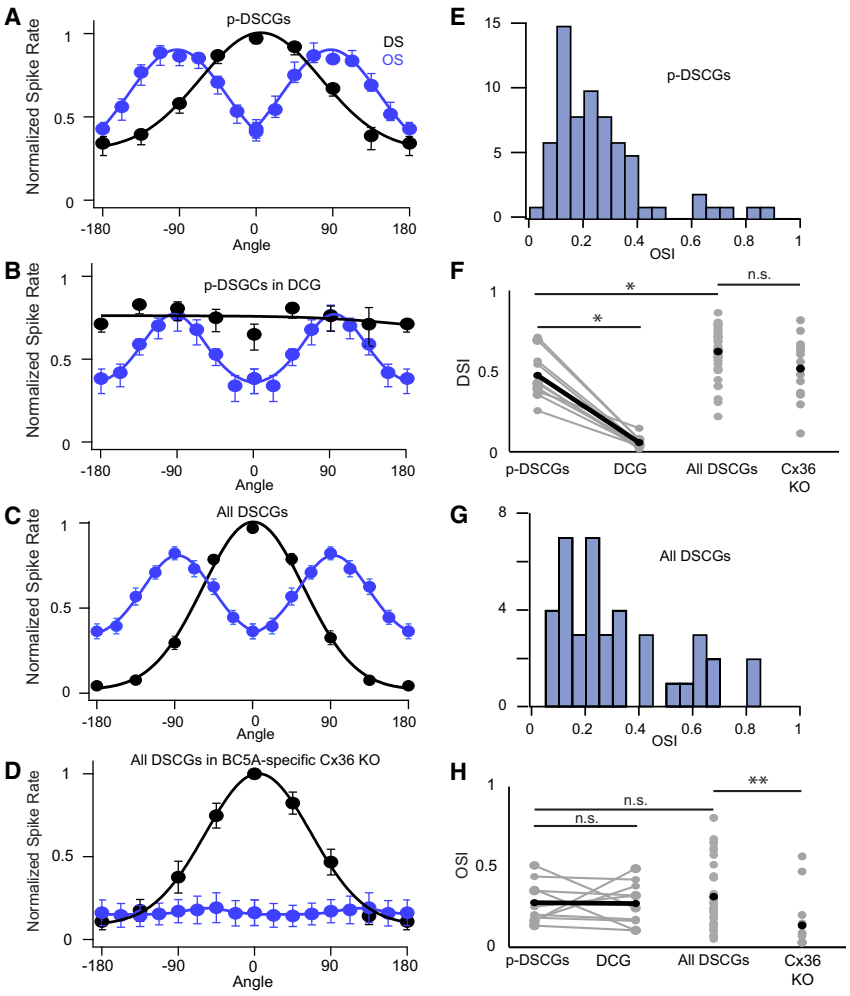

Figure 5. Orientation and direction selectivity in DSGCs are driven by distinct synaptic mechanisms

(A) Tuning curves constructed from the spiking responses from TRHR + p-DSGCs evoked by moving (black) or static (blue) bars (eight directions or orientations). Note, that the DSGCs respond best to vertical bars that are orthogonal to their preferred-null motion axis.

(B) Blocking starburst amacrine cell output using a mGluR2 receptor agonist (DCG-IV) abolishes direction selectivity but leaves orientation selectivity intact.

(C) Tuning curves constructed from the spiking responses from all four populations of ON-OFF DSGCs evoked by moving (black) or static (blue) bars (eight directions or orientations).

(D) Conditional CX36 KO in KCNG4-Cre abolishes the responses to oriented bars across all populations of DSGCs, consistent with the effects of the KO on BC5As (Figures 2A–2D). However, responses to small moving spots remain direction selective, similar to control.

(E and G) Distribution of OSI values recorded from TRHR + p-DSGCs (E, n = 52) and from all four subtypes of ON-OFF DSGCs (G, n = 40) in control conditions (difference between TRHR + p-DSGCs and all DSGCs is not significant [n.s.]).

(F and H) Average DSI and OSI values for different conditions. p-DSGCs (n = 10), DCG-IV (n = 10), all DSGCs (n = 40), and CX36 KO (n = 13). Manipulations that disrupt starburst amacrine cell function (DCG) abolish direction selectivity but have little effect on orientation selectivity. By contrast, knocking out CX36 in BC5As disrupts orientation selectivity while leaving direction selectivity in DSGCs relatively intact (note that orientation selectivity in the OFF pathway is still observed in the BC5A-specific CX36-KO; Figure S2). *$p < 0.005$, **$p < 0.05$, calculated as paired (DCG) or unpaired t test.

In the general population of ON-OFF DSGCs that we identified "blindly" based on their ON-OFF responses and their direction-selective tuning properties, we observed an orientation selectivity that was similar to that of TRHR + p-DSGCs (Figures 5C, 5G, and 5H). Moreover, the preferred orientation was always orthogonal to the DSGC's preferred-null axis (defined by moving stimuli). As DSGCs were not genetically identified, the cardinal direction each cell encoded was not clear in these experiments, and tuning properties were averaged across the entire population (Figure 5C).

Interestingly, orientation selectivity was not present in any of the DSGCs when CX36 was deleted quite selectively in BC5As in the KCNG4^{Cre} × Gjd2$^{fl/fl}$ mouse retina (Figures 5D and 5H), which we have shown eliminates BC5A orientation tuning and induces suppressive responses to large bars (Figure 2). In contrast, the directional-tuning properties of DSGCs in this mouse line appeared to be intact (Figure 5D). Furthermore, orientation selectivity was observed in the OFF responses of these ganglion cells, which were apparent in roughly half the recorded DSGCs (Figure S2), confirming the ON specificity of the genetic manipulation. Together, these results suggest that gap junction mechanisms, possibly between BC5A and WF5A, play a central role in enabling DSGCs to detect the orientation of features in the visual world, although how they contribute to orientation tuning in superior/inferior DSGCs remains to be examined.

DISCUSSION

In this study, we demonstrated that the axonal terminals of BC5A respond best to vertically oriented bars, a response property that appears to rely on an asymmetric pattern of electrical coupling. In addition, synaptic inputs to BC5A terminal arbors arise overwhelmingly from processes of a single type of WF ACs that are also oriented along the vertical axis, raising the possibility that these may serve as the prejunctional partners. Finally, orientation-selective information appears to be faithfully transferred to downstream ganglion cells, including posterior-coding DSGCs, which in turn can relay this feature to higher visual centers. Together, these newly defined circuit specializations support the notion that in the mouse visual system, the vertical axis may represent a key reference axis along which visual information can be organized.[60]

Mechanisms of orientation selectivity in BC terminals

Classic studies in the visual cortex suggest that the integration of information from neurons with symmetrical RFs along a single axis gives rise to orientation selectivity.[61,62] In the retina, a variety of inhibitory ACs, as well as a few types of output ganglion cells, harbor dendritic processes that extend out along the horizontal or vertical axes, making them orientation selective. Orientation-selective ACs play an important role in shaping feature selectivity in a select set of OSGCs by providing pre- and postsynaptic inhibition.[45,63–65] Puzzlingly, however, orientation-tuned excitatory inputs remain tuned in the presence of inhibitory receptor blockers, indicating that additional excitatory mechanisms may also shape orientation tuning.

Here, based on several lines of function evidence, we propose that the electrical coupling of BC terminals to vertically oriented AC dendrites modify their output properties and serve as the substrate for orientation-tuned glutamatergic input to third-order neurons. First, we found that BC terminals integrated visual information over several hundred microns, far larger than their dendritic fields. Second, BC excitation could be driven by stimuli outside the BC RF, requiring lateral connections. Third, orientation selectivity persisted under ionotropic glutamate receptor blockade, which provides another strong indication that gap junctions play an important role in its generation.[46,47,66,67] The loss of the extended spatial integration observed in the BC5A-specific CX36 KO further supports this notion. The current results suggest that CX36 plays a pivotal role in shaping BC5A feature selectivity.

BC terminals are known to be directly coupled to each other, as well as select narrow-field ACs including AII and A8 ACs.[12,28,30,31,68–70] Such coupling, in some cases, may almost double the size of BC RFs.[10,29] Consistent with this notion, we found that BC5A terminal RF dimensions along the horizontal axis were ~twice the size expected based on their dendritic fields. However, along the vertical axis, BC terminals integrate information over distances ~4 times those spanned by their dendritic field (or even greater distances when chemical synapses are blocked; Figure S3). This is more difficult to explain by BC-to-BC coupling as it requires that the coupling to be asymmetric, occurring preferentially along the vertical axis; there is no evidence for such anisotropy. Recently, BC5As in the rabbit retina were also found to be electrically coupled to another AC, which remains to be identified (ACx[26]). Here, we propose that BC5A terminals are electrically coupled to the vertical processes of the WF ACs that were revealed in this study, i.e., the WF5As.

Electrical coupling between WF AC processes and BC5A terminals would be expected to promote spatial integration along the vertical axis since they are vertically oriented. There is evidence that WF ACs harbor mixed electrical/chemical synapses,[71] which is a common motif that is observed in inhibitory circuits in other brain areas.[72] Moreover, a recent report demonstrates that vertically oriented AC processes confer orientation selectivity upon certain ganglion cells via gap junctions,[73] setting strong precedence for the proposed mechanism. Also, we reasoned that if GABAergic inhibition was the dominant signal from these oriented WF5A processes, then we might have expected BC terminals to be tuned along the horizontal axis, and this tuning would be sensitive to ionotropic glutamate receptor antagonists, which we did not observe experimentally.

DSGCs encode orientation and direction

DSGCs have been extensively studied over the past 60 years, and thus it is somewhat surprising that their orientation-selective properties have been previously overlooked. There are several reasons why this might be the case. First, classic studies demonstrated that orientation information is conveyed by specialized OSGCs that are distinct from DSGCs. Thus, much of the initial effort aimed at understanding how these features are extracted tended to be directed to specific cell types, i.e., studies probing the mechanisms underlying direction selectivity focused on DSGCs and mechanisms underlying orientation selectivity focused on OSGCs (reviewed by Antinucci and Hindges,[45] Mauss et al.,[74] and Vaney et al.[75]).

Second, gap junctions are known to be experimentally labile and regulated by ambient light levels, which may make orientation selectivity harder to characterize.[76–78] The targeted optical approaches used here greatly facilitated measurements and enabled orientation-selective responses to be measured in relatively "fresh" retinas. In addition, retinas were maintained under relatively dark-adapted conditions where the level of gap junction coupling may be maximal.[76] It is also worth pointing out that in many recent studies, only part of the retina is stimulated, either because the retinas are hemisected before being placed in the recording chamber or because the light stimuli are presented through a 40× or 60× objective, which only covers the classical RFs of the cell. These studies would miss the orientation selectivity that develops through longer-range connections. Finally, a few studies carried out in both mouse and rabbit retina did note orientation selectivity in certain DSGCs. However, a systematic relationship between the directional and orientation axes was not observed, negating the idea that these features were multiplexed.[79,80] By contrast, here we show that the orientation selectivity in all types of DSGCs is always orthogonal to the preferred-null motion axis. This makes DSGCs similar to other direction-selective neurons in downstream visual areas that tend to have an orientation preference orthogonal to their preferred-null axis, similar to what we have described here.

Mechanistically, orientation and direction selectivity might be expected to be linked as they both rely on an asymmetric inhibitory RF. However, here we found that pharmacologically or genetically blocking starburst ACs, which are required for direction selectivity, did not affect orientation selectivity, at least for the p-DSGC subtype. Interestingly, a recent structure/function study of layer 2/3 (L2/3) pyramidal neurons in the visual cortex also indicates that orientation and direction selectivity may be shaped by distinct circuit mechanisms.[81]

Limitations of the study

The idea that Cx36-containing gap junctions between WF5A and BC5A terminals play a critical role in generating orientation selectivity is based on two lines of indirect evidence. Orientation selectivity in BC5A terminals persists in the presence of glutamate receptor antagonists but is abolished when gap junctions are genetically deleted in these cells (using the KCNG4^{Cre} × Gjd2$^{fl/fl}$ mouse line[34]). In theory, it is possible that

the developmental impact of the Cx36 deletion or the pharmacology may affect other aspects of the circuit and prevent the expression of orientation selectivity. Unfortunately, we could not directly detect gap junction plaques between BC5A and WF5As in the current dataset.[51] Higher-resolution transmission electron microscopy, which can be used to visualize gap junctions,[26,71] will be needed to directly confirm the electrical coupling between WF amacrine processes and BC5A terminals. Regardless of the precise electrical and/or chemical nature of their synaptic connection, the highly asymmetric distribution of the WF amacrine processes and their profuse connectivity to BC5A terminals strongly suggest that they contribute to orientation selectivity.

Another limitation of this study is that the proposed circuit mechanism underlying vertical orientation selectivity in DSGCs applies only to the sets encoding posterior or anterior motion. For superior/inferior coding DSGCs that have a horizontal tuning preference (orthogonal to their preferred-null axis), the mechanisms are less clear. It is possible that other BCs in the circuit are horizontally tuned and selectively drive these DSGCs and not the posterior or anterior DSGCs. Arguing against this prospect, however, anatomical studies suggest that overlapping sets of BCs drive the four types of ON-OFF DSGCs that encode the cardinal directions.[6,51] It is also possible that inhibitory mechanisms contribute to orientation selectivity in superior/inferior coding DSGCs by sign inverting the vertically tuned signals arising from BC5A and/or other BC types in the circuit. A more comprehensive analysis of the spiking, sources of synaptic input, and anatomical connectivity patterns of other types of DSGCs and BCs will resolve the apparent mismatch between functional and anatomical results.

Conclusions

In the natural scene, there is a strong bias toward vertically oriented edges (such as trees or blades of grass[60]), and thus it is not surprising that there is also a bias for vertical orientation selectivity in the visual system.[19,82–84] However, although widely observed, the functional advantage of orientation and direction encoded by the same neuron remains to be firmly established. One possibility is that mechanisms that shape orientation selectivity serve to sharpen the directional tuning properties of DSGCs, as has been observed for DS neurons in the fly retina.[85] Alternatively, the processing of visual information through vertically oriented filters (i.e., removal of the horizontal image components) may simplify the task of encoding the direction by posterior-coding ganglion cells and enable animals to navigate more efficiently through their natural environments.

STAR★METHODS

Detailed methods are provided in the online version of this paper and include the following:

- KEY RESOURCES TABLE
- RESOURCE AVAILABILITY
  - Lead contact
  - Materials availability
  - Data and code availability
- EXPERIMENTAL MODEL AND SUBJECT DETAILS
  - Animals
- METHOD DETAILS
  - Retinal preparations
  - Visual stimulation
  - Sharp-electrode electroporation
  - 2-Photon image acquisition
  - Calcium imaging analysis
- QUANTIFICATION AND STATISTICAL ANALYSIS

SUPPLEMENTAL INFORMATION

Supplemental information can be found online at https://doi.org/10.1016/j.celrep.2023.112030.

ACKNOWLEDGMENTS

We would like to thank Dr. Marla Feller for TRHR-EGFP mice and Dr. David Paul for the Gjd2$^{fl/fl}$ mice, Dr. Jamie Boyd and Dr. Benjamin Murphy-Baum for their help with 2P imaging and analysis software (IGOR, Wavemetrics), Mike Delsey for technical support, and Tracy Michaels for assistance with animal care and breeding. This work was supported by CIHR 159444 (G.B.A.).

AUTHOR CONTRIBUTIONS

Conceptualization, L.H. and G.B.A.; data collection, L.H. and P.R.-C.; formal analysis, L.H., P.R.-C., and D.B.; writing, L.H. and G.B.A.; software, L.H.; SBEM analysis, D.B.; review & editing, D.B.; supervision, G.B.A.; funding acquisition, G.B.A.

DECLARATION OF INTERESTS

The authors declare no competing interests.

Received: May 25, 2022
Revised: November 8, 2022
Accepted: January 10, 2023
Published: January 24, 2023

REFERENCES

1. Franke, K., Berens, P., Schubert, T., Bethge, M., Euler, T., and Baden, T. (2017). Inhibition decorrelates visual feature representations in the inner retina. Nature *542*, 439–444. https://doi.org/10.1038/nature21394.
2. Schreyer, H.M., and Gollisch, T. (2021). Nonlinear spatial integration in retinal bipolar cells shapes the encoding of artificial and natural stimuli. Neuron *109*, 1692–1706.e8. https://doi.org/10.1016/j.neuron.2021.03.015.
3. Wässle, H., Puller, C., Müller, F., and Haverkamp, S. (2009). Cone contacts, mosaics, and territories of bipolar cells in the mouse retina. J. Neurosci. *29*, 106–117. https://doi.org/10.1523/JNEUROSCI.4442-08.2009.
4. Euler, T., Haverkamp, S., Schubert, T., and Baden, T. (2014). Retinal bipolar cells: elementary building blocks of vision. Nat. Rev. Neurosci. *15*, 507–519. https://doi.org/10.1038/nrn3783.
5. Shekhar, K., Lapan, S.W., Whitney, I.E., Tran, N.M., Macosko, E.Z., Kowalczyk, M., Adiconis, X., Levin, J.Z., Nemesh, J., Goldman, M., et al. (2016). Comprehensive classification of retinal bipolar neurons by single-cell transcriptomics. Cell *166*, 1308–1323.e30. https://doi.org/10.1016/j.cell.2016.07.054.
6. Helmstaedter, M., Briggman, K.L., Turaga, S.C., Jain, V., Seung, H.S., and Denk, W. (2013). Connectomic reconstruction of the inner plexiform layer in the mouse retina. Nature *500*, 168–174. https://doi.org/10.1038/nature12346.

7. Baden, T., Berens, P., Bethge, M., and Euler, T. (2013). Spikes in mammalian bipolar cells support temporal layering of the inner retina. Curr. Biol. *23*, 48–52. https://doi.org/10.1016/j.cub.2012.11.006.

8. Werblin, F.S., and Dowling, J.E. (1969). Organization of the retina of the mudpuppy, Necturus macubsus. II. Intracellular recording. J. Neurophysiol. *32*, 339–355.

9. Kaneko, A. (1973). Receptive field organization of bipolar and amacrine cells in the goldfish retina. J. Physiol. *235*, 133–153.

10. Hare, W.A., and Owen, W.G. (1990). Spatial organization of the bipolar cell's receptive field in the retina of the tiger salamander. J. Physiol. *421*, 223–245.

11. Borges, S., and Wilson, M. (1987). Structure of the receptive fields of bipolar cells in the salamander retina. J. Neurophysiol. *58*, 1275–1291.

12. Dacey, D., Packer, O.S., Diller, L., Brainard, D., Peterson, B., and Lee, B. (2000). Center surround receptive field structure of cone bipolar cells in primate retina. Vision Res. *40*, 1801–1811.

13. Awatramani, G.B., and Slaughter, M.M. (2000). Origin of transient and sustained responses in ganglion cells of the retina. J. Neurosci. *20*, 7087–7095.

14. Ichinose, T., Fyk-Kolodziej, B., and Cohn, J. (2014). Roles of ON cone bipolar cell subtypes in temporal coding in the mouse retina. J. Neurosci. *34*, 8761–8771. https://doi.org/10.1523/JNEUROSCI.3965-13.2014.

15. Devries, S.H. (2000). Bipolar cells use kainate and AMPA receptors to filter visual information into separate channels. Neuron *28*, 847–856.

16. Gollisch, T., and Meister, M. (2010). Eye smarter than scientists believed: neural computations in circuits of the retina. Neuron *65*, 150–164. https://doi.org/10.1016/j.neuron.2009.12.009.

17. Grimes, W.N., Schwartz, G.W., and Rieke, F. (2014). The synaptic and circuit mechanisms underlying a change in spatial encoding in the retina. Neuron *82*, 460–473. https://doi.org/10.1016/j.neuron.2014.02.037.

18. Matsumoto, A., Agbariah, W., Nolte, S.S., Andrawos, R., Levi, H., Sabbah, S., and Yonehara, K. (2021). Direction selectivity in retinal bipolar cell axon terminals. Neuron *109*, 2928–2942.e8. https://doi.org/10.1016/j.neuron.2021.07.008.

19. Johnston, J., Seibel, S.H., Darnet, L.S.A., Renninger, S., Orger, M., and Lagnado, L. (2019). A retinal circuit generating a dynamic predictive code for oriented features. Neuron *102*, 1211–1222.e3. https://doi.org/10.1016/j.neuron.2019.04.002.

20. Tachibana, M., and Kaneko, A. (1987). y-Aminobutyric acid exerts a local inhibitory action on the axon terminal of bipolar cells: evidence for negative feedback from amacrine cells. Proc. Natl. Acad. Sci. USA *84*, 3501–3505.

21. Lukasiewicz, P.D., and Werblin, F.S. (1994). A novel GABA receptor modulates synaptic transmission from bipolar to ganglion and amacrine cells in the tiger salamander retina. J. Neurosci. *14*, 1213–1223.

22. Eggers, E.D., Mccall, M.A., Lukasiewicz, P.D., and Lukasiewicz, P.D. (2007). Presynaptic inhibition differentially shapes transmission in distinct circuits in the mouse retina. J. Physiol. *582*, 569–582. https://doi.org/10.1113/jphysiol.2007.131763.

23. Yan, W., Laboulaye, M.A., Tran, N.M., Whitney, I.E., Benhar, I., and Sanes, J.R. (2020). Mouse retinal cell atlas: molecular identification of over sixty amacrine cell types. J. Neurosci. *40*, 5177–5195. https://doi.org/10.1523/JNEUROSCI.0471-20.2020.

24. Demb, J.B., and Singer, J.H. (2015). Functional circuitry of the retina. Annu. Rev. Vis. Sci. *1*, 263–289. https://doi.org/10.1146/annurev-vision-082114-035334.

25. Yadav, S.C., Tetenborg, S., and Dedek, K. (2019). Gap junctions in A8 amacrine cells are made of connexin36 but are differently regulated than gap junctions in AII amacrine cells. Front. Mol. Neurosci. *12*, 99. https://doi.org/10.3389/fnmol.2019.00099.

26. Sigulinsky, C.L., Anderson, J.R., Kerzner, E., Rapp, C.N., Pfeiffer, R.L., Rodman, T.M., Emrich, D.P., Rapp, K.D., Nelson, N.T., Lauritzen, J.S., et al. (2020). Network architecture of gap junctional coupling among parallel processing channels in the mammalian retina. J. Neurosci. *40*, 4483–4511. https://doi.org/10.1523/JNEUROSCI.1810-19.2020.

27. Kerstein, P.C., Leffler, J., Sivyer, B., Taylor, W.R., and Wright, K.M. (2020). Gbx2 identifies two amacrine cell subtypes with distinct molecular, morphological, and physiological properties. Cell Rep. *33*, 108382. https://doi.org/10.1016/j.celrep.2020.108382.

28. Kuo, S.P., Schwartz, G.W., and Rieke, F. (2016). Nonlinear spatiotemporal integration by electrical and chemical synapses in the retina. Neuron *90*, 320–332. https://doi.org/10.1016/j.neuron.2016.03.012.

29. Zhang, A.-J., and Wu, S.M. (2009). Receptive fields of retinal bipolar cells are mediated by heterogeneous synaptic circuitry. J. Neurosci. *29*, 789–797. https://doi.org/10.1523/JNEUROSCI.4984-08.2009.

30. Saito, T., and Kujiraoka, T. (1988). Characteristics of bipolar-bipolar coupling in the carp retina. J. Gen. Physiol. *91*, 275–287.

31. Arai, I., Tanaka, M., and Tachibana, M. (2010). Active roles of electrically coupled bipolar cell network in the adult retina. J. Neurosci. *30*, 9260–9270. https://doi.org/10.1523/JNEUROSCI.1590-10.2010.

32. Asari, H., and Meister, M. (2014). The projective field of retinal bipolar cells and its modulation by visual context. Neuron *81*, 641–652. https://doi.org/10.1016/j.neuron.2013.11.029.

33. Greene, M.J., Kim, J.S., and Seung, H.S.; EyeWirers (2016). Analogous convergence of sustained and transient inputs in parallel on and off pathways for retinal motion computation. Cell Rep. *14*, 1892–1900. https://doi.org/10.1016/j.celrep.2016.02.001.

34. Duan, X., Krishnaswamy, A., De la Huerta, I., and Sanes, J.R. (2014). Type II cadherins guide assembly of a direction-selective retinal circuit. Cell *158*, 793–807. https://doi.org/10.1016/j.cell.2014.06.047.

35. Jain, V., Murphy-Baum, B.L., deRosenroll, G., Sethuramanujam, S., Delsey, M., Delaney, K.R., and Awatramani, G.B. (2020). The functional organization of excitation and inhibition in the dendrites of mouse direction-selective ganglion cells. Elife *9*, e52949. https://doi.org/10.7554/eLife.52949.

36. Hanson, L., Sethuramanujam, S., de Rosenroll, G., Jain, V., and Awatramani, G.B. (2019). Retinal direction selectivity in the absence of asymmetric starburst amacrine cell responses. Elife *8*, e42392. https://doi.org/10.7554/eLife.42392.

37. Sethuramanujam, S., McLaughlin, A.J., DeRosenroll, G., Hoggarth, A., Schwab, D.J., and Awatramani, G.B. (2016). A central role for mixed acetylcholine/GABA transmission in direction coding in the retina. Neuron *90*, 1243–1256. https://doi.org/10.1016/j.neuron.2016.04.041.

38. Yonehara, K., Farrow, K., Ghanem, A., Hillier, D., Balint, K., Teixeira, M., Jüttner, J., Noda, M., Neve, R.L., Conzelmann, K.K., and Roska, B. (2013). The first stage of cardinal direction selectivity is localized to the dendrites of retinal ganglion cells. Neuron *79*, 1078–1085. https://doi.org/10.1016/j.neuron.2013.08.005.

39. Park, S.J.H., Kim, I.J., Looger, L.L., Demb, J.B., and Borghuis, B.G. (2014). Excitatory synaptic inputs to mouse on-off direction- selective retinal ganglion cells lack direction tuning. J. Neurosci. *34*, 3976–3981. https://doi.org/10.1523/JNEUROSCI.5017-13.2014.

40. Krieger, B., Qiao, M., Rousso, D.L., Sanes, J.R., and Meister, M. (2017). Four alpha ganglion cell types in mouse retina: function, structure, and molecular signatures. PLoS One *12*, e0180091. https://doi.org/10.1371/journal.pone.0180091.

41. Hoggarth, A., McLaughlin, A.J., Ronellenfitch, K., Trenholm, S., Vasandani, R., Sethuramanujam, S., Schwab, D., Briggman, K.L., and Awatramani, G.B. (2015). Specific wiring of distinct amacrine cells in the directionally selective retinal circuit permits independent coding of direction and size. Neuron *86*, 276–291. https://doi.org/10.1016/j.neuron.2015.02.035.

42. Gaynes, J.A., Budoff, S.A., Grybko, M.J., Hunt, J.B., and Poleg-Polsky, A. (2022). Classical center-surround receptive fields facilitate novel object detection in retinal bipolar cells. Nat. Commun. *13*, 5575. https://doi.org/10.1038/s41467-022-32761-8.

43. Strauss, S., Korympidou, M.M., Ran, Y., Franke, K., Schubert, T., Baden, T., Berens, P., Euler, T., and Vlasits, A.L. (2022). Center-surround interactions underlie bipolar cell motion sensitivity in the mouse retina. Nat. Commun. *13*, 5574. https://doi.org/10.1038/s41467-022-32762-7.

44. Srivastava, P., deRosenroll, G., Matsumoto, A., Michaels, T., Turple, Z., Jain, V., Sethuramanujam, S., Murphy-Baum, B.L., Yonehara, K., and Awatramani, G.B. (2022). Spatiotemporal properties of glutamate input support direction selectivity in the dendrites of retinal starburst amacrine cells. Elife *11*, e81533. https://doi.org/10.7554/elife.81533.

45. Antinucci, P., and Hindges, R. (2018). Orientation-selective retinal circuits in vertebrates. Front. Neural Circuits *12*, 11. https://doi.org/10.3389/fncir.2018.00011.

46. Farrow, K., Teixeira, M., Szikra, T., Viney, T.J., Balint, K., Yonehara, K., and Roska, B. (2013). Ambient illumination toggles a neuronal circuit switch in the retina and visual perception at cone threshold. Neuron *78*, 325–338. https://doi.org/10.1016/j.neuron.2013.02.014.

47. Münch, T.A., da Silveira, R.A., Siegert, S., Viney, T.J., Awatramani, G.B., and Roska, B. (2009). Approach sensitivity in the retina processed by a multifunctional neural circuit. Nat. Neurosci. *12*, 1308–1316. https://doi.org/10.1038/nn.2389.

48. Nakajima, Y., Iwakabe, H., Akazawa, C., Nawa, H., Shigemoto, R., Mizuno, N., and Nakanishi, S. (1993). Molecular characterization of a novel retinal metabotropic glutamate receptor mGluR6 with a high agonist selectivity for L-2-amino-4- phosphonobutyrate. J. Biol. Chem. *268*, 11868–11873. https://doi.org/10.1016/s0021-9258(19)50280-0.

49. Slaughter, M.M., and Miller, R.F. (1983). Bipolar cells in the mudpuppy retina use an excitatory amino acid neurotransmitter. Nature *303*, 537–538.

50. Behrens, C., Schubert, T., Haverkamp, S., Euler, T., and Berens, P. (2016). Connectivity map of bipolar cells and photoreceptors in the mouse retina. Elife *5*, e20041. https://doi.org/10.7554/eLife.20041.

51. Ding, H., Smith, R.G., Poleg-Polsky, A., Diamond, J.S., and Briggman, K.L. (2016). Species-specific wiring for direction selectivity in the mammalian retina. Nature *535*, 105–110. https://doi.org/10.1038/nature18609.

52. Badea, T.C., and Nathans, J. (2004). Quantitative analysis of neuronal morphologies in the mouse retina visualized by using a genetically directed reporter. J. Comp. Neurol. *480*, 331–351. https://doi.org/10.1002/cne.20304.

53. Lin, B., and Masland, R.H. (2006). Populations of wide-field amacrine cells in the mouse retina. J. Comp. Neurol. *499*, 797–809. https://doi.org/10.1002/cne.21126.

54. Kim, I.J., Zhang, Y., Yamagata, M., Meister, M., and Sanes, J.R. (2008). Molecular identification of a retinal cell type that responds to upward motion. Nature *452*, 478–482. https://doi.org/10.1038/nature06739.

55. Rousso, D.L., Qiao, M., Kagan, R.D., Yamagata, M., Palmiter, R.D., and Sanes, J.R. (2016). Two pairs of on and off retinal ganglion cells are defined by intersectional patterns of transcription factor expression. Cell Rep. *15*, 1930–1944. https://doi.org/10.1016/j.celrep.2016.04.069.

56. Sabbah, S., Gemmer, J.A., Bhatia-Lin, A., Manoff, G., Castro, G., Siegel, J.K., Jeffery, N., and Berson, D.M. (2017). A retinal code for motion along the gravitational and body axes. Nature *546*, 492–497. https://doi.org/10.1038/nature22818.

57. Mainen, Z.F., Malinow, R., and Svoboda, K. (1999). Synaptic calcium transients in single spines indicate that NMDA receptors are not saturated. Nature *399*, 151–155.

58. Nath, A., and Schwartz, G.W. (2016). Cardinal orientation selectivity is represented by two distinct ganglion cell types in mouse retina. J. Neurosci. *36*, 3208–3221. https://doi.org/10.1523/JNEUROSCI.4554-15.2016.

59. Sethuramanujam, S., Awatramani, G.B., and Slaughter, M.M. (2018). Cholinergic excitation complements glutamate in coding visual information in retinal ganglion cells. J. Physiol. *596*, 3709–3724. https://doi.org/10.1113/JP275073.

60. Coppola, D.M., Purves, H.R., McCoy, A.N., and Purves, D. (1998). The distribution of oriented contours in the real world. Proc. Natl. Acad. Sci. USA *95*, 4002–4006. https://doi.org/10.1073/pnas.95.7.4002.

61. Hubel, D.H., and Wiesel, T.N. (1959). Receptive fields of single neurones in the cat's striate cortex. J. Physiol. *148*, 574–591.

62. Hubel, D.H., and Wiesel, A.T.N. (1962). Receptive fields, binocular interaction and functional architecture in the Cat's visual cortex. J. Physiol. *160*, 106–154.

63. Venkataramani, S., and Taylor, W.R. (2016). Synaptic mechanisms generating orientation selectivity in the on pathway of the rabbit retina. J. Neurosci. *36*, 3336–3349. https://doi.org/10.1523/JNEUROSCI.1432-15.2016.

64. Venkataramani, S., and Taylor, W.R. (2010). Orientation selectivity in rabbit retinal ganglion cells is mediated by presynaptic inhibition. J. Neurosci. *30*, 15664–15676. https://doi.org/10.1523/JNEUROSCI.2081-10.2010.

65. Murphy-Baum, B.L., and Taylor, W.R. (2015). The synaptic and morphological basis of orientation selectivity in a polyaxonal amacrine cell of the rabbit retina. J. Neurosci. *35*, 13336–13350. https://doi.org/10.1523/JNEUROSCI.1712-15.2015.

66. van Wyk, M., Wässle, H., and Taylor, W.R. (2009). Receptive field properties of ON-and OFF-ganglion cells in the mouse retina. Vis. Neurosci. *26*, 297–308. https://doi.org/10.1017/S0952523809990137.

67. Manookin, M.B., Beaudoin, D.L., Ernst, Z.R., Flagel, L.J., and Demb, J.B. (2008). Disinhibition combines with excitation to extend the operating range of the off visual pathway in daylight. J. Neurosci. *28*, 4136–4150. https://doi.org/10.1523/JNEUROSCI.4274-07.2008.

68. Lee, S.C.S., Meyer, A., Schubert, T., Hüser, L., Dedek, K., and Haverkamp, S. (2015). Morphology and connectivity of the small bistratified A8 amacrine cell in the mouse retina. J. Comp. Neurol. *523*, 1529–1547. https://doi.org/10.1002/cne.23752.

69. Mills, S.L., and Massey, S.C. (1995). Differential properties of two gap junctional pathways made by AII amacrine cells. Nature *377*, 734–737.

70. Tsukamoto, Y., and Omi, N. (2017). Classification of mouse retinal bipolar cells: type-specific connectivity with special reference to rod-driven AII amacrine pathways. Front. Neuroanat. *11*, 92. https://doi.org/10.3389/fnana.2017.00092.

71. Marc, R.E., Sigulinsky, C.L., Pfeiffer, R.L., Emrich, D., Anderson, J.R., and Jones, B.W. (2018). Heterocellular coupling between amacrine cells and ganglion cells. Front. Neural Circuits *12*, 90. https://doi.org/10.3389/fncir.2018.00090.

72. Fukuda, T., and Kosaka, T. (2000). Gap junctions linking the dendritic network of GABAergic interneurons in the Hippocampus. J. Neurosci. *20*, 1519–1528.

73. Nath, A., and Schwartz, G.W. (2017). Electrical synapses convey orientation selectivity in the mouse retina. Nat. Commun. *8*, 2025. https://doi.org/10.1038/s41467-017-01980-9.

74. Mauss, A.S., Vlasits, A., Borst, A., and Feller, M. (2017). Visual circuits for direction selectivity. Annu. Rev. Neurosci. *40*, 211–230. https://doi.org/10.1146/annurev-neuro-072116.

75. Vaney, D.I., Sivyer, B., and Rowland Taylor, W. (2012). Direction selectivity in the retina: symmetry and asymmetry in structure and function. Nat. Rev. Neurosci. *13*, 194–208. https://doi.org/10.1038/nrn3165.

76. Roy, S., and Field, G.D. (2019). Dopaminergic modulation of retinal processing from starlight to sunlight. J. Pharmacol. Sci. *140*, 86–93. https://doi.org/10.1016/j.jphs.2019.03.006.

77. Bloomfield, S.A., and Völgyi, B. (2009). The diverse functional roles and regulation of neuronal gap junctions in the retina. Nat. Rev. Neurosci. *10*, 495–506. https://doi.org/10.1038/nrn2636.

78. Baldridge, W.H., Vaney, D.I., and Weiler, R. (1998). The modulation of intercellular coupling in the retina. Semin. Cell Dev. Biol. *9*, 311–318. https://doi.org/10.1006/scdb.1998.0235.

79. He, S., Levick, W.R., and Vaney, D.I. (1998). Distinguishing direction selectivity from orientation selectivity in the rabbit retina. Vis. Neurosci. *15*, 439–447. https://doi.org/10.1017/S0952523898153038.

80. Baden, T., Berens, P., Franke, K., Román Rosón, M., Bethge, M., and Euler, T. (2016). The functional diversity of retinal ganglion cells in the mouse. Nature *529*, 345–350. https://doi.org/10.1038/nature16468.

81. Weiler, S., Guggiana Nilo, D., Bonhoeffer, T., Hübener, M., Rose, T., and Scheuss, V. (2022). Orientation and direction tuning align with dendritic morphology and spatial connectivity in mouse visual cortex. Curr. Biol. *32*, 1743–1753.e7. https://doi.org/10.1016/j.cub.2022.02.048.

82. Rivlin-Etzion, M., Zhou, K., Wei, W., Elstrott, J., Nguyen, P.L., Barres, B.A., Huberman, A.D., and Feller, M.B. (2011). Transgenic mice reveal unexpected diversity of On-Off direction selective retinal ganglion cell subtypes and brain structures involved in motion processing. J. Neurosci. *31*, 8760–8769. https://doi.org/10.1523/JNEUROSCI.0564-11.2011.

83. Zhao, X., Chen, H., Liu, X., and Cang, J. (2013). Orientation-selective responses in the mouse lateral geniculate nucleus. J. Neurosci. *33*, 12751–12763. https://doi.org/10.1523/JNEUROSCI.0095-13.2013.

84. Girshick, A.R., Landy, M.S., and Simoncelli, E.P. (2011). Cardinal rules: visual orientation perception reflects knowledge of environmental statistics. Nat. Neurosci. *14*, 926–932. https://doi.org/10.1038/nn.2831.

85. Fisher, Y.E., Silies, M., and Clandinin, T.R. (2015). Orientation selectivity sharpens motion detection in Drosophila. Neuron *88*, 390–402. https://doi.org/10.1016/j.neuron.2015.09.033.

86. Yao, X., Cafaro, J., McLaughlin, A.J., Postma, F.R., Paul, D.L., Awatramani, G., and Field, G.D. (2018). Gap junctions contribute to differential light adaptation across direction-selective retinal ganglion cells. Neuron *100*, 216–228.e6. https://doi.org/10.1016/j.neuron.2018.08.021.

87. Murphy-Baum, B.L., and Awatramani, G.B. (2022). Parallel processing in active dendrites during periods of intense spiking activity. Cell Rep. *38*, 110412. https://doi.org/10.1016/j.celrep.2022.110412.

88. Wei, W., Elstrott, J., and Feller, M.B. (2010). Two-photon targeted recording of GFP-expressing neurons for light responses and live-cell imaging in the mouse retina. Nat. Protoc. *5*, 1347–1352. https://doi.org/10.1038/nprot.2010.106.

STAR★METHODS

KEY RESOURCES TABLE

REAGENT or RESOURCE	SOURCE	IDENTIFIER
Chemicals, peptides, and recombinant proteins		
X-Rhod-5F	Molecular Probes	CAT# X23984
Sulforhodamine-101	Sigma	CAT# S7635
Alexa Fluor 488 Hydrazide	ThermoFisher	CAT# A10436
Tetrodotoxin	Alomone	CAT# t550
D-AP5	Alomone	CAT# D-145
UBP-310	Abcam	CAT# ab120336
CNQX disodium salt	Tocris	CAT# 1045
DCG-IV	Tocris	CAT# 975
TPMPA	Tocris	CAT# 1040
QX-314 chloride	Tocris	CAT# 2313
SR-95531 Hydrobromide	HelloBio	CAT# HB0901
Experimental models: Organisms/strains		
Mouse: wild type (C57BL/6J)	The Jackson Laboratory	RRID: IMSR_JAX:000664
Mouse: TRHR-eGFP	Dr. Marla Feller, UC Berkeley	RRID: MMRRC_030036-UCD
Mouse: Kcng4-cre	The Jackson Laboratory	(B6.129(SJL)-Kcng4$^{tm1.1(cre)Jrs/J}$, JAX stock #029414
Mouse: GCaMP6f	The Jackson Laboratory	(B6J.Cg-Gt(ROSA)26Sor$^{tm95.1(CAG-GCaMP6f)Hze/MwarJ}$ JAX stock #028865
Mouse: Gjd2$^{fl/fl}$	Dr. David Paul, Harvard	(Yao et al., 2018)[86]
Software and algorithms		
MATLAB	Mathworks	http://www.mathworks.com; RRID: SCR_01622
Igor Pro	WaveMetrics	RRID: SCR_000325
pClamp	Molecular Devices	RRID:SCR_011323
StimGen	(Jain et al., 2020)[35]	https://github.com/benmurphybaum/StimGen; https://doi.org/10.5281/zenodo.5903691
NeuroTools	(Murphy-Baum et al., 2022)[87]	https://github.com/benmurphybaum/NeuroTools; https://doi.org/10.5281/zenodo.5903694
KNOSSOS	N/A	http://www.knossostool.org; RRID:SCR_003582

RESOURCE AVAILABILITY

Lead contact

Dr. Gautam B Awatramani (gautam@uvic.ca).

Materials availability

This study did not generate any unique reagents. Further information and requests for resources and reagents should be directed to and will be fulfilled by the lead contact.

Data and code availability

- All data reported in this paper will be shared by the lead contact upon request.
- There are no original codes generated in this paper.
- Any additional information required to reanalyze the data reported in this paper is available from the lead contact upon request

EXPERIMENTAL MODEL AND SUBJECT DETAILS

Animals

All animal procedures were performed in accordance with the Canadian Council on Animal Care (CCAC) and approved by the University of Victoria's Animal Care Committee. Mice of both sexes, aged between P21-P140 were used for experiments. Animals were group-housed in a 12-h dark/light cycle.

Experiments were performed using TRHR-eGFP (provided by Dr. Marla Feller, UC Berkeley; RRID: MMRRC_030036-UCD) for posterior DSGC recordings. For calcium imaging, the KCNG4-Cre mice (B6.129(SJL)-Kcng4$^{tm1.1(cre)Jrs/J}$, JAX stock #029414) were crossed with mice carrying a transgene for Cre-dependent expression of the calcium indicator GcaMP6f (Ai95D:B6J.Cg-Gt(ROSA)26Sor$^{tm95.1(CAG-GcaMP6f)Hze/MwarJ}$, JAX stock #028865). To investigate the role of electrical coupling, a triple transgenic was generated by crossing KCNG4-Cre x GcaMP6f$^{fl/fl}$ x Gjd2$^{fl/fl}$ line.[86] To disrupt GABA release from starburst amacrine cells, the ChAT-Cre mouse line (RRID: MGI_5475195) was crossed with a mouse strain carrying a floxed allele of Slc32a1 (*Slc32a1*^{tm1Lowl}, JAX stock # 012897).

METHOD DETAILS

Retinal preparations

Prior to retina extraction, mice were dark-adapted for 45–60 min to optimize light-evoked responses. Mice were anesthetized with isoflurane and euthanized by cervical dislocation. Then the retina was extracted and dissected in Ringer's solution (110 mM NaCl, 2.5 mM KCl, 1 mM $CaCl_2$, 1.6 mM $MgCl_2$, 10 mM glucose, and 22 mM $NaHCO_3$) under dim red light. The retina was mounted on a 0.22 mm membrane filter (Millipore) with a pre-cut square window approximately 2 mm^2 in size through which the stimulus was projected onto the retina. The retina was viewed with infrared light using a Spot RT3 CCD camera (Diagnostic Instruments) mounted on an upright Olympus BX51 WI fluorescent microscope equipped with a 40x water immersion lens (Olympus Canada). Throughout the experiment, the retina was continuously perfused with warmed (~37°C) Ringer's solution bubbled with carbogen (5% CO_2:95% O_2). For each experiment, the nasal axis of the retina was marked with a small cut.[88] The orientation of the retina was varied across days to ensure that the orientation selectivity we observed was not due to any potential bias in the experimental setup. For extracellular recordings, electrodes were pulled to 3–6 MΩ and filled with Ringer's solution. CNQX and DCG-IV were purchased from Tocris, TTX and D-AP5 were purchased from Alomone, and UBP-310 was purchased from Abcam.

Visual stimulation

Light stimuli, produced using a digital light projector equipped with a 450 nm LED, were focused onto the outer segments of the photoreceptors using the sub-stage condenser. Visual stimuli were created in the MATLAB environment (Psychtoolbox). For measuring orientation-selectivity, 50 μm × 500 μm bars were presented in 8 orientations. For DS measurements, 100 μm spots moving at 1000 μm/s in 8 directions were used. Surround stimuli consisted of a 50 μm × 500 μm bar overlayed with a 50 μm × 50 μm black mask in the center. Increasing bars had a width of 50 μm and a length ranging from 50–500 μm. All stimuli were presented over a dark background. The luminance was measured to be approximately 10 photoisomerizations/rod/s (R*/s) for control conditions and was increased up to10-fold during CNQX + UBP-310 application or Cx36 KO conditions.

Sharp-electrode electroporation

To visualize single bipolar or ganglion cells, sharp electrodes (80–120 mΩ) were backfilled with 15 mM of sulforhodamine-101 (SR-101, Sigma Aldrich) and then brought into contact with the cell of interest. Iontophoresis was achieved by applying the pulse function in the MultiClamp 700B software (Molecular Devices) set at 50 ms[51].

2-Photon image acquisition

For measuring Ca^{2+} signals mediated by NMDA receptors, $TRHR^+$ DSGCs were voltage-clamped ~0 mV using 3–5 MΩ electrodes containing the calcium indicator X-Rhod-5F (500 μM, Life Technologies). A high chloride electrode solution was used (E_{Cl^-} ~ 0 mV; 110 mM CsCl, 1 mM MgSO4, 10 mM EGTA, 10 mM HEPES, 5 mM QX-314). This ensured that no sizable inhibitory or excitatory light-evoked synaptic currents were generated during the imaging experiment (Vhold ~0 mV) thereby decreasing the potential voltage-clamp artifacts associated with large currents. Imaging was initiated approximately 20 min after break-in, which allowed the calcium indicator to adequately fill the DSGC dendrites.

For bipolar cell calcium imaging, the KCNG4-Cre x GcaMP6f mouse line was used with or without conditional CX36KO. To ensure imaging was performed in the proper retinal layer, DSGCs were identified by their characteristic spiking responses to motion and then filled with a red dye (sulforhodamine-101) via sharp electrode electroporation (see above) to visualize the dendritic arbor while calcium responses were recorded from labeled bipolar cell terminals in green (Figure 1B).

Two-photon excitation was delivered using a Mai Tai Ti:Sapphire laser (Spectra Physics) tuned to 920 nm, guided by X/Y galvanometer mirrors (Cambridge Technology). Image scans were acquired using custom software developed by Dr. Jamie Boyd

(University of British Columbia) in the Igor Pro environment. To prevent the light stimulus from contaminating the fluorescent response, the LED projector used for presenting light stimuli was synchronized with the mirror turn-around signal. The PMT signals were digitized at 1 MHz (PCI-6110, National Instruments) for image formation.

Calcium imaging analysis

All imaging analysis was performed using custom-written software by Dr. Benjamin Murphy-Baum in IGOR pro.[87] ROIs of approximately 3 μm were drawn around individual terminals or regions of dendrites and the signals were smoothed using a 2nd order Savitzky-Golay filter. Peak ΔF/F values were calculated for each ROI. During the application of pharmacology, the same ROIs were used across conditions.

QUANTIFICATION AND STATISTICAL ANALYSIS

DSI and OSI were calculated as the amplitude of the vector sum:

$$DSI = \frac{\sum R(\theta)e^{i\theta}}{\sum R(\theta)} \quad OSI = \frac{\sum R(\theta)e^{2i\theta}}{\sum R(\theta)}$$

where R(θ) is the response for θ direction or orientation calculated from the peak spike rate. The preferred angle was calculated from the resultant (DSI) or half phase of the resultant (OSI) of the vector sum. DSI or OSI ranged from 0 to 1, with 0 indicating a perfectly symmetrical response, and 1 indicating a response in only one of eight directions or orientations presented.

Population data have been expressed as mean ± SEM and are indicated in the figure legend along with the sample size. Student's t-test (paired or unpaired depending on the samples) was used to compare values under different conditions, * indicates $p < 0.005$, ** indicates $p < 0.05$.

Cell Reports, Volume *42*

Supplemental information

Hierarchical retinal computations rely on hybrid chemical-electrical signaling

Laura Hanson, Prathyusha Ravi-Chander, David Berson, and Gautam B. Awatramani

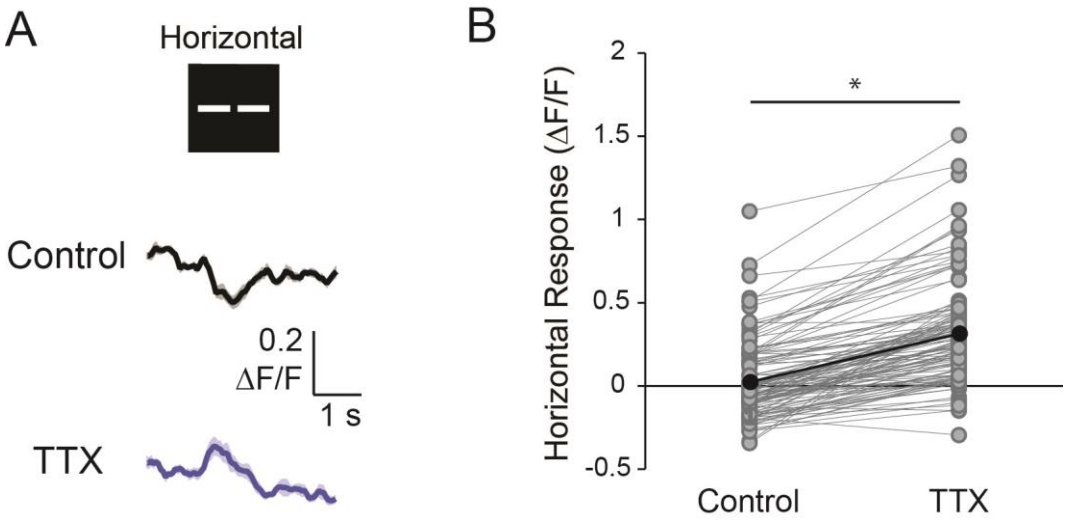

Supplementary Figure 1, Related to Figure 2. TTX disrupts surround inhibition

(A) Calcium responses observed in BC5A terminals during surround activation along the horizontal axis results in a decrease in the calcium signal observed under control conditions (black) in ~half of the ROIs (68 of 123) with only small responses in the remaining ROIs, indicating strong surround inhibition. TTX (blue) disrupts the surround inhibition, causing an increase (119 of 123 ROIs) in the response during horizontal surround stimuli.

(B) Responses across the population to surround stimuli along the horizontal axis in control and TTX, grey is individual ROIs, and black is the average (n=7).

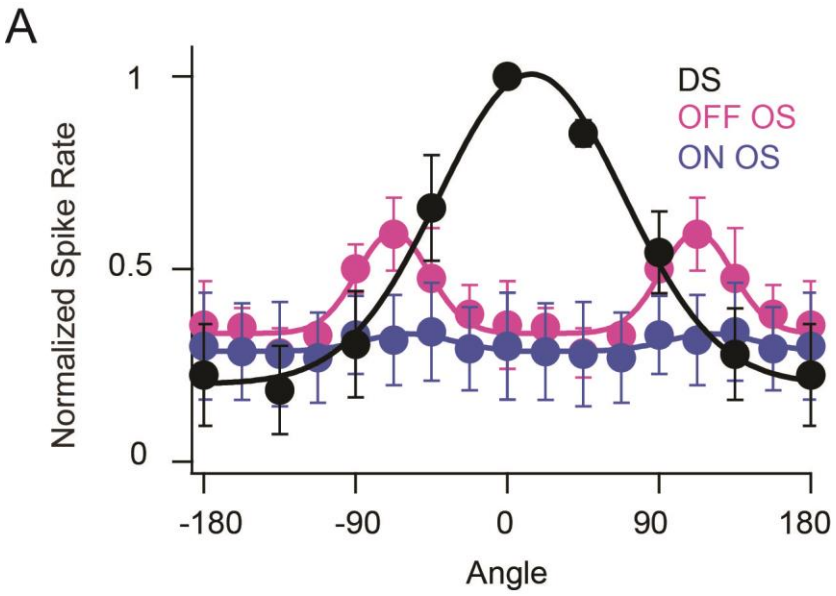

Supplementary Figure 2, Related to Figure 5. Connexin36 KO disrupts ON but not OFF responses

(A) Tuning curves constructed from the spiking responses recorded from ON-OFF DSGCs in the CX36 KO in KCNG4-Cre abolish the ON responses to large stationary stimuli (ON OS, blue) while the OFF responses remain intact (OFF OS, magenta). Robust ON responses can be evoked using moving stimuli (DS<, black), indicating the specificity of the CX36 KO to the BC5A (n=4).

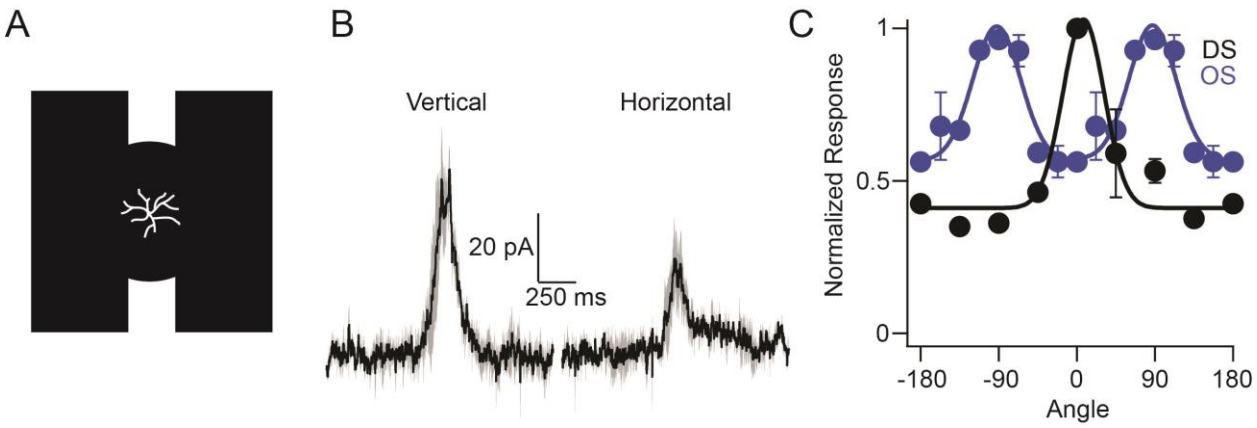

Supplementary Figure 3, Related to Figure 5. DSGCs receive asymmetric glutamate inputs from the surround

(A) Surround excitation to TRHR+ ON-OFF DSGCs was measured using vertical or horizontal bars with a 600 µm mask centered over the receptive field.

(B) EPSCs measure at +40 mV in SR, TPMPA, CNQX, and UBP-310 to isolate the NMDA responses. Glutamatergic excitation can be driven from the far surround and is stronger when stimulated along the vertical axis compared to the horizontal axis.

(C) NMDA responses evoked from the surround (OS, blue) are orthogonal to the preferred direction of motion (DS, black), matching the relationship observed during spiking responses without a mask (**Figure 5A**) (n=2). Also see Asari and Meister (2014).

	Bipolar Cell Inputs	
	WF(5A)	WF(7)
5A	**38%**	5%
5B	34%	1%
5C	27%	-
5D	12%	1%
6	2%	10%
7	2%	**81%**
8	-	1%
4	-	-

	Bipolar Cell Outputs	
	WF(5A)	WF(7)
5A	**70%**	2%
5B	4%	-
5C	10%	-
5D	1%	-
6	10%	24%
7	3%	**74%**
8	-	1%
4	1%	-

	Weighting of outputs by class	
	WF(5A)	WF(7)
BCs	n=597 (52%)	n=286 (60%)
ACs	n=383 (33%)	n=176 (37%)
RGCs	n=167 (15%)	n=11 (2%)

	Amacrine Cell Outputs	
	WF(5A)	WF(7)
WF(5A)	42%	-
WF(7)	6%	60%
ON SAC	18%	-
SFE-like OIA/OIB-linked	7%	-
VGluT3	6%	10%
CRH-1	4%	10%
H21	4%	-
nGnG	-	10%
Gbx2	-	10%
Identified	84 (22%)	10 (6%)
Unidentified	215 (78%)	166 (94%)

	RGC outputs	
	WF(5A)	WF(7)
lambda 5oi	42%	-
lambda 5t	3%	4%
F-mini ON	39%	30%
ON DS	10%	-
ON-OFF DS	-	4%
OIB	9%	-
W3 (UHD)	8%	-
OIA	6%	-
R-cell (ON-delayed)	4&	7%
SBC(1)	-	11%
SBC(2)	4%	-
EW25(rho)	-	11%
M2(8)	-	22%
M4(sON alpha)	-	4%
M5(PixON)	-	4%
Identified	139 (83%)	27 (82%)
Unidentified	28 (17%)	6 (18%)

Supplementary Table 1, Related to Figure 3. Wide-field amacrine cells synaptic inputs and outputs based on connectomic reconstructions

Example T5A with all AC inputs mapped		
#1	Total	113
	WF(5A)	**34**
	ON SAC	2
	H16	1
	H36	1
	H40	1
	VIP/RAC2(RB)	1
	Unidentified	71
#2	Total	89
	WF(5A)	**53**
	WF(7)	3
	WF(5t)	2
	WF other	5
	TH2	2
	VIP/RAC2(RB)	2
	Unidentified	22
#3	Total	76
	WF(5A)	**5**
	Other	1
	Unidentified	70

Example T7 with all AC inputs mapped		
#1	Total	148
	WF(7)	**68**
	CRH-1	5
	WF(6)	4
	H52	1
	Unidentified	70

Supplementary Table 2, Related to Figure 3. Amacrine cell inputs to individual type 5A and type 7 bipolar cells